Strengthening Mechanisms of 15 vol.% Al$_2$O$_3$ Nanoparticles Reinforced Aluminum Matrix Nanocomposite Fabricated by High Energy Ball Milling and Vacuum Hot Pressing

Ke Zhao[1,2] · Zhongying Duan[1,2] · Jinling Liu[1,2] · Guozheng Kang[1,2] · Linan An[3]

Abstract

Increasing nanoparticle volume fraction has been proved to be effective in improving the strength of nanoparticle reinforced Al matrix nanocomposite. However, the underlying mechanisms for the ultrahigh strength of those nanocomposites with high volume fraction (> 10 vol.%) nanoparticles are short of experimental research. In this study, the strengthening mechanisms of high strength Al matrix nanocomposite reinforced with 15 vol.% Al$_2$O$_3$ nanoparticles were investigated experimentally and analyzed theoretically. The results show that the thermal mismatch induced geometrically necessary dislocations exhibit a negligible strengthening effect, because of their low density in the nanocomposite that is contradiction to the conventional dislocation punch model. Orowan mechanism makes a major strengthening contribution in view of the deformation process dominated by nanoparticle-dislocation interactions due to the extreme pinning effect of nanoparticles on dislocation motion. In addition, the several mechanisms including grain boundary strengthening, load transfer strengthening, and elastic modulus mismatch induced dislocation strengthening contribute to the strength increase.

Keywords Al matrix nanocomposite · Strengthening mechanism · Nanoparticle · High volume fraction · Microstructure

1 Introduction

Nanoparticles reinforced Al matrix nanocomposites have attracted much attention for their high strength without sacrificing the ductility, as well as super wear, creep, and fatigue performance [1–3], which render them potential candidates in automobile, military, and aerospace industries. It is well established that the mechanical properties of this kind of nanocomposites rely heavily on the diameter, volume fraction, and distribution of nanoparticles in the matrix. Specifically, the strength increases with the increase in particle

volume fraction and/or the decrease in particle size under the prerequisite of uniform distribution of nanoparticles in the matrix [4–7]. However, currently there are still few excellent research works on the structural and mechanical behavior of uniformly dispersed Al matrix nanocomposites with nanoparticle volume fraction above 10 vol.%, due to the fact that nanoparticles are badly prone to agglomerate from the effect of their extremely huge surface area [8–10], and introduce more flaws such as cracks and porosity into the nanocomposites [8], leading to reduction in strength and ductility of the nanocomposites.

A variety of methods have been developed so far to overcome the aforementioned difficulty, such as high energy ball milling [4, 11–13], ultrasonically casting [14], friction stir processing [15], accumulative roll bonding [16], etc. Among all types of fabrication methods, high energy ball milling has become one of the most promising methods for achieving uniform distribution of high volume fraction nanoparticles in metal matrix [11–13]. It has been demonstrated in our previous works [12, 13] that 15 vol.% Al$_2$O$_3$ nanoparticles can be evenly distributed in the Al matrix by such method, also the resultant nanocomposite exhibits ultrahigh strength under quasistatic and dynamic compression, while

✉ Ke Zhao
    zhaooke@163.com

1   School of Mechanics and Engineering, Southwest Jiaotong University, Chengdu 610031, China

2   Applied Mechanics and Structure Safety Key Laboratory of Sichuan Province, Southwest Jiaotong University, Chengdu 610031, China

3   Department of Materials Science and Engineering, University of Central Florida, Orlando, FL 32816, USA

the microstructure and strengthening mechanisms of such nanocomposite remain unclear up to now.

In general, the strengthening mechanisms of Al matrix nanocomposites with nanoparticle volume fraction lower than 10% are as follows: (i) load transfer strengthening [7], (ii) grain refinement strengthening resulted from the inhibiting effect of nanoparticles on grain growth of Al matrix [2, 4], (iii) dislocation strengthening due to the coefficient of thermal expansion (CTE) mismatch and elastic modulus (EM) mismatch between metal matrix and hard nanoparticles [16], and (iv) Orowan strengthening [17], whereby dislocations encounter the nonshearable nanoparticles and bow out. Among them Orowan strengthening makes a major contribution to strength increase [9]. By using analytical models, Guo et al. [15] and Lin et al. [18] proposed that Orowan strengthening is still the main strengthening mechanism when the nanoparticles volume fraction reaches up to 14% and 35%, respectively, nevertheless, it has not been proved by experiments. Moreover, the strength of the nanocomposite with 15 vol.% Al_2O_3 nanoparticles reported in our preview work [12] is much higher than that of the nanocomposite with 14 vol.% nanoparticles reported by Guo et al. [15] and of the nanocomposite with 17 vol.% nanoparticles reported by Lin et al. [18], which is pretty hard to be explained by using existing analytical models.

In this study, it is concerned with the microstructure, strengthening mechanisms of the Al matrix nanocomposite containing 15 vol.% Al_2O_3 nanoparticles that was fabricated via the same process as in previous work [12], but in which the Al_2O_3 nanoparticles have a relatively larger size (~86 nm). The several mechanisms including grain boundary strengthening, load transfer strengthening, dislocation strengthening, and Orowan strengthening were experimentally examined and discussed. The results shown that interactions between nanoparticles and dislocations and subsequent dislocation rearrangement dominate the deformation process, indicating that the strength increase is mainly attributed to the Orowan strengthening, in agreement with the associated theoretical analysis.

2 Experimental

Pure Al powder with average size of ~74 µm (Shanghai Shanpu Ltd., China) and Al_2O_3 powder with average size of 85 nm (Hefei Zhonghang Nanotechnology Development Co., Ltd., China) were used as raw materials. The Al matrix nanocomposite containing 15 vol.% Al_2O_3 nanoparticles was fabricated via high energy ball milling followed by vacuum hot pressing. Firstly, the raw powder mixes were ball milled in a high energy planetary ball mill with WC grinding media for 20 h in Ar atmosphere at rotation speed of 240 r/min. The Ball-powder mass ratio was maintained

at 25:1, 4 wt% ethonal was used as a process control agent. The milled powder mixes were then hot pressed at 620 °C for 50 min under a uniaxial pressure of 50 MPa. The pure Al sample was prepared by same conditions for comparison. The relative density of both of these materials was measured to be > 99% by means of Archimedes method.

X-ray diffraction (XRD, Rigaku-D/max-2400, Japan) was conducted to identify phases of the nanocomposite, scanning electron microscope (SEM, JMS-7800F, JEOL, Japan), and transmission electron microscope (TEM, JEM-2100F, JEOL, Japan) operating at 200 kV were used to characterize the microstructures of the as-produced and post-deformation nanocomposite. Compression tests were carried out using an Instron 2367 universal testing machine at a strain rate of 1×10^{-3}/s. The compressive specimens with size of $\Phi 3$ mm $\times 6$ mm were cut from hot pressed compacts.

3 Results and Discussion

Figure 1a shows the true stress–strain curves of the as-produced nanocomposite as well as that of pure Al. As can be seen that, the nanocomposite has a yield strength of 536 MPa, ~11 times higher than that of pure Al, as well as maximum strength reaching 730 MPa, indicating that the high volume fraction of Al_2O_3 nanoparticles gives rise to a significant strengthening effect to the Al matrix. Moreover, the nanocomposite exhibits a rapid and brief hardening at the early stage of the deformation followed by a linear work softening, as illustrated in Fig. 1b. It is worth emphasizing that this nanocomposite achieves the excellent combination of the high strength and good strain, and the maximum strength is higher than other pure Al matrix composites reinforced with high volume fraction nano-/submicro-/microparticles reported in the literature [5, 18–26].

In order to uncover the underlying mechanisms for strengthening of high volume fraction Al_2O_3 nanoparticles in Al matrix, the microstructures of the nanocomposite before and after deformation were examined in detail. As can be seen in Fig. 2a, the as-produced nanocomposite is fully densified, with no evident flaws such as porosity and cracks being observed, also the nanoparticles are randomly and uniformly distributed in the Al matrix and have a size distribution ranging from 24 to 130 nm, with an average value of ~86 nm. This indicates a fully densified homogeneous microstructure feature of the nanocomposite. Furthermore, XRD analysis of the as-produced nanocomposite (Fig. 2b) shows that only Al and α-Al_2O_3 phases are detected, suggesting that there is little or no impurity phase such as oxides and carbides that is generally formed in the composite during high energy ball milling and subsequent sintering process. This implies that the strengthening contribution arose from impurity phases can be ignored.
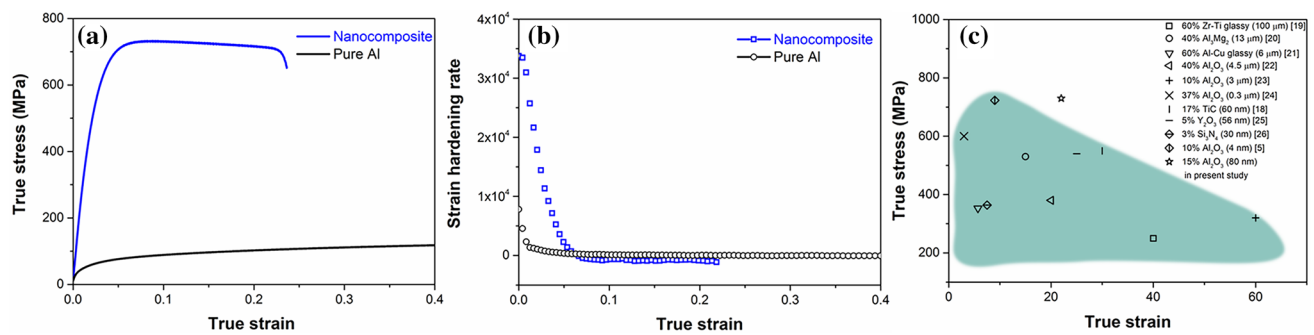
Fig. 1 **a**, **b** Compressive true stress–strain curves and corresponding strain hardening rate-true strain curves of the as-produced nanocomposite and pure Al, respectively. **c** Maximum strength versus strain for the current nanocomposite in comparison with those of typical conventionally strengthened Al matrix composites
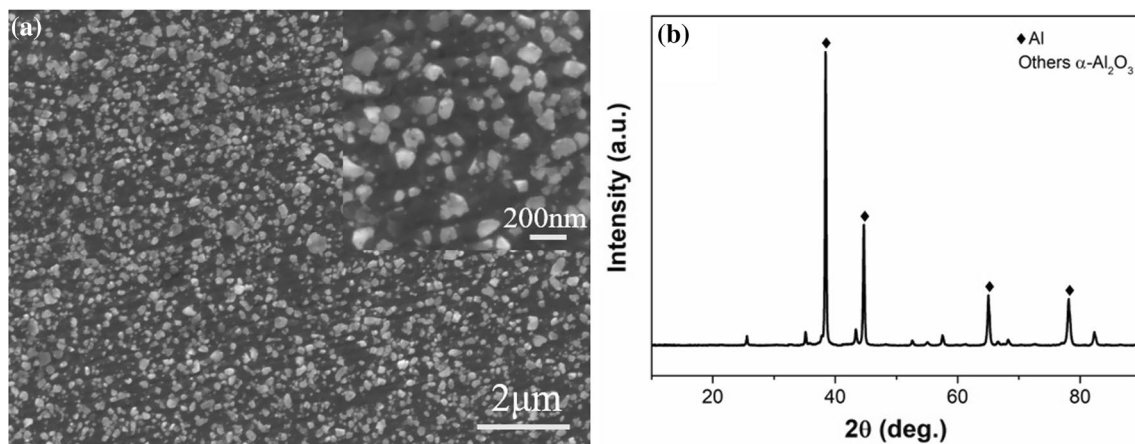

Fig. 2 Typical SEM images **a**, and XRD pattern **b** of the as-produced nanocomposite

Figure 3a presents the TEM image of the as-produced nanocomposite, it can be seen that the Al grain size is of micrometer scale, and the nanoparticles indicated by white arrows are located both inside Al grains and near grain boundaries, this further verifies the uniform distribution of nanoparticles thorough Al matrix. The micrometer-scaled Al grains can further be confirmed by indexing selected area electron diffraction (SAED) pattern corresponding to Fig. 3a. As illustrated in Fig. 3b, the SAED pattern exhibits the single-crystal diffraction reflections originated from Al matrix and polycrystalline diffraction rings derived from randomly oriented Al₂O₃ nanoparticles. The average grain size of Al matrix was calculated to be 1.8 μm on the basis of statistical grain numbers attained from more than ten of TEM images. In general, the Al grains with ultrafine or nano size are maintained during the thermomechanical powder consolidation process thanks to the significant pinning effect of nanoparticles on the grain boundary motion [2, 3]. The excessive grain growth in this study may be associated with the application of high sintering temperature which can greatly promotes grain growth. The increase of the yield

strength due to the grain boundary strengthening can be estimated by Hall–Petch equation [27], as given below: $\Delta\sigma_G = k_y d^{-1/2}$, where k_y is the Hall–Petch coefficient, 0.06 MPa m$^{1/2}$ for pure Al, and d is the grain size.

It is well documented that the particle/matrix interface character is critical to the performance of the composites. As shown in Fig. 3c, the interface between Al₂O₃ nanoparticle and Al matrix is metallurgically clean without any flaws or additional phases, indicating a strong interfacial bonding which allows effective load transfer from the matrix to the nanoparticles and thus the improved strength. Here, a modified shear lag model [7] was used to account for the transfer of load from Al matrix to Al₂O₃ nanoparticles via shear stresses. In light of nearly cubic shape of the Al₂O₃ nanoparticles employed in this study, the strengthening due to load transfer can be estimated by [7]: $\Delta\sigma_L = 0.5\sigma_m V_p$, where σ_m represents the yield strength of pure Al, and V_p refers to the volume fraction of nanoparticles.

Because of the CTE mismatch between the hard particle and the soft metal matrix, the geometrically necessary dislocations (GNDs) near the particle/matrix interface will be
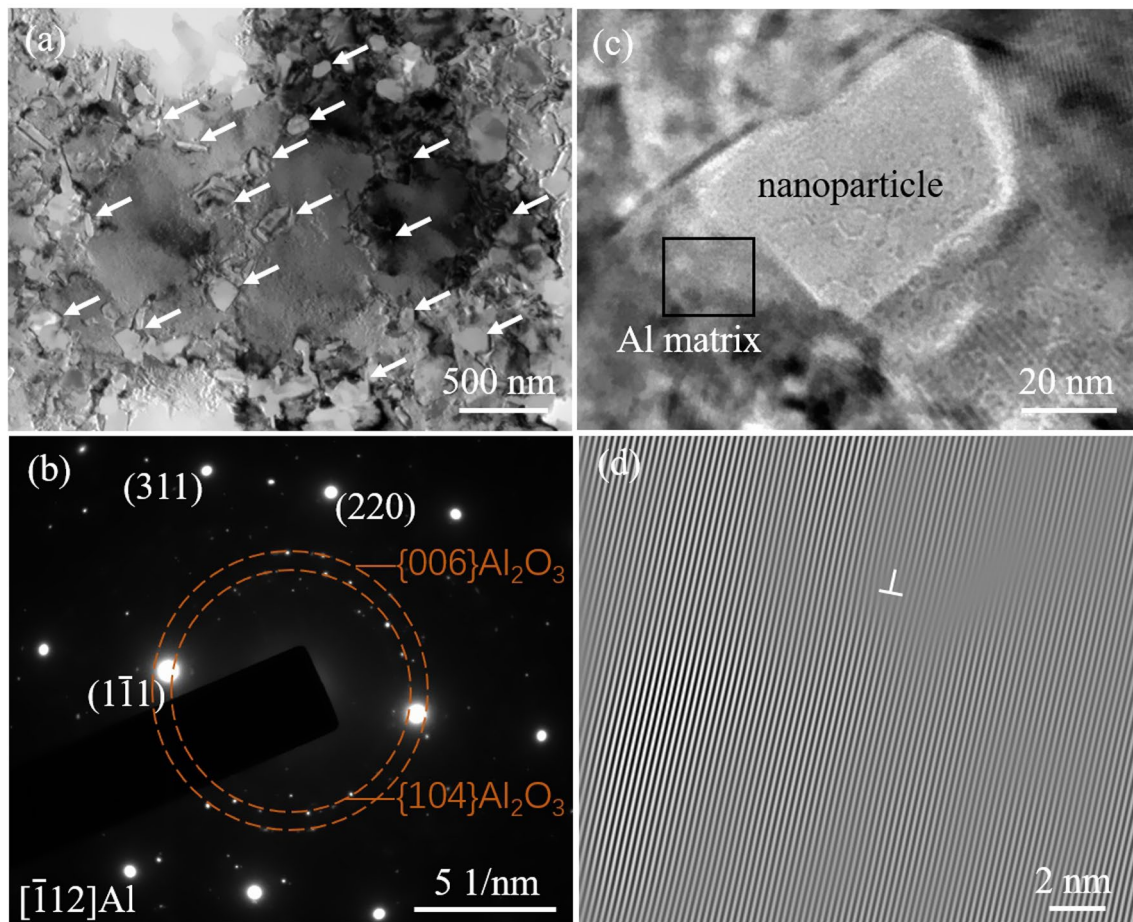
Fig. 3 **a** Typical TEM image ,**b** corresponding SAED pattern of the as-produced nanocomposite, **c** TEM image of nanoparticle/matrix interface, **d** IFFT image of the area marked by black rectangle in **c**

punched out into the Al matrix to relax the thermal stress when the composite is cooled down from the processing temperature. According to the theory of Arsenault et al. [28], the GND density due to CTE mismatch can be estimated by the following equation [29]: $\rho_{GND}^{CTE} = \frac{12V_P\Delta\alpha\Delta T}{(1-V_P)bd_P}$, where $\Delta\alpha = 16.7\times 10^{-6}$ K^{-1} is the CTE mismatch between the Al matrix and Al$_2$O$_3$ nanoparticles, d_P is the particle size, $b = 0.286$ nm is the Burgers vector of pure Al, ΔT is the difference between the processing temperature and room temperature. According to this equation, the CTE mismatch induced GND density would increase as decreasing particle size and/or increasing the particle volume fraction. This has been verified to be valid in several investigations [29–31]. For analysis of the nanocomposite in present study, $\Delta T = 250$K was taken in view of the maximum temperature at which CTE mismatch is relaxed by dislocation punching is 550 K [30], and then the ρ_{GND}^{CTE} was calculated to be 2.4×10^{15} m^{-2}. However, TEM image (Fig. 3a) shows that there seems only a small amount of dislocations indicated by red arrows in the

Al matrix even in the vicinity of Al$_2$O$_3$ nanoparticles, which is contradicted to the predicted density value of GNDs due to CTE mismatch. To inspect the correctness of this point, the CTE mismatch induced GNDs density was measured by using an inverse fast Fourier transformation (IFFT) for the region being close to the Al$_2$O$_3$ nanoparticle. For instance, as illustrated in Fig. 3d, IFFT for the region marked by the black rectangle in Fig. 3c shows few edge dislocations marked by T near the Al$_2$O$_3$ nanoparticle. As such, the density of GNDs in the vicinity of Al$_2$O$_3$ nanoparticles was determined to be 6.5×10^{12} m^{-2} based on tens of IFFT images, three orders of magnitude lower than previously predicted, implying that it is improper to predict the CTE mismatch induced GNDs by using dislocation punching model as the nanoparticles at a given diameter exceeds a certain critical volume fraction. This discrepancy can be explained by referencing dislocation annihilation mechanism proposed by Redsten et al. [30]. In particular, the GND loops are punched out under the drive of the thermal stress caused by CTE mismatch and further form multiple pile-ups (i.e.,

the GND punched zone) around the nanoparticles. As the thermal mismatch strain increases with the extension of cooling down of the nanocomposite, the size of the GND punched zone increases. When the GND punched zones from neighboring nanoparticles overlap with each other, annihilation of the GND loops of opposite sign is expected to take place, leading to decrease in GND density. Whether the GND punched zones overlap with each other or not depends on not only the volume fraction of nanoparticles but also the particle size, due to the fact that the interparticle distance decreases as increasing volume fraction and/or decreasing particle size. Redsten et al. [30] proposed that the strengthening by CTE induced GND loops is not expected when the particle size is smaller than a critical diameter d^*, the d^* can be estimated as $d^* = \frac{b}{\Delta\alpha\Delta T}$. As for the case of 15 vol.% Al₂O₃ nanoparticles reinforced Al matrix nanocomposite evaluated in this study, the d^* can be calculated to be 68.5 nm, which is smaller than the size of Al₂O₃ nanoparticles, meaning that the GND loops can be punched out around the Al₂O₃ nanoparticles. Whereas, the interparticle distance determined by both the volume fraction of particles and particle size concurrently is reduced to a certain value

at which GND punched zones overlap with each other between Al₂O₃ nanoparticles. Besides that, the interparticle distance is smaller than the particle size, which is beneficial for interaction between GND loops from neighboring nanoparticles and then the occurrence of GND loops annihilation.

Apart from the CTE mismatch induced GNDs, GND would be generated in the Al matrix to accommodate the strain incompatibility around the nanoparticles due to the EM mismatch between Al and nanoparticles [32], when the nanocomposite is plastically deformed, namely EM mismatch induced GNDs. These GNDs can effectively trap the secondary dislocations during plastic deformation of the nanocomposite, a high density of dislocations are piled up around the nanoparticles. As can be seen in TEM images of post-deformation nanocomposite (Fig. 4), dislocation tangles are observed at the border between Al₂O₃ nanoparticle (indicated by white arrow) and Al matrix, which is in stark contrast to that before deformation. Also, the dislocation density is found to increase closer to the Al₂O₃ nanoparticle. One should be noted that the high density of dislocations near the Al₂O₃ nanoparticle may also result from interaction
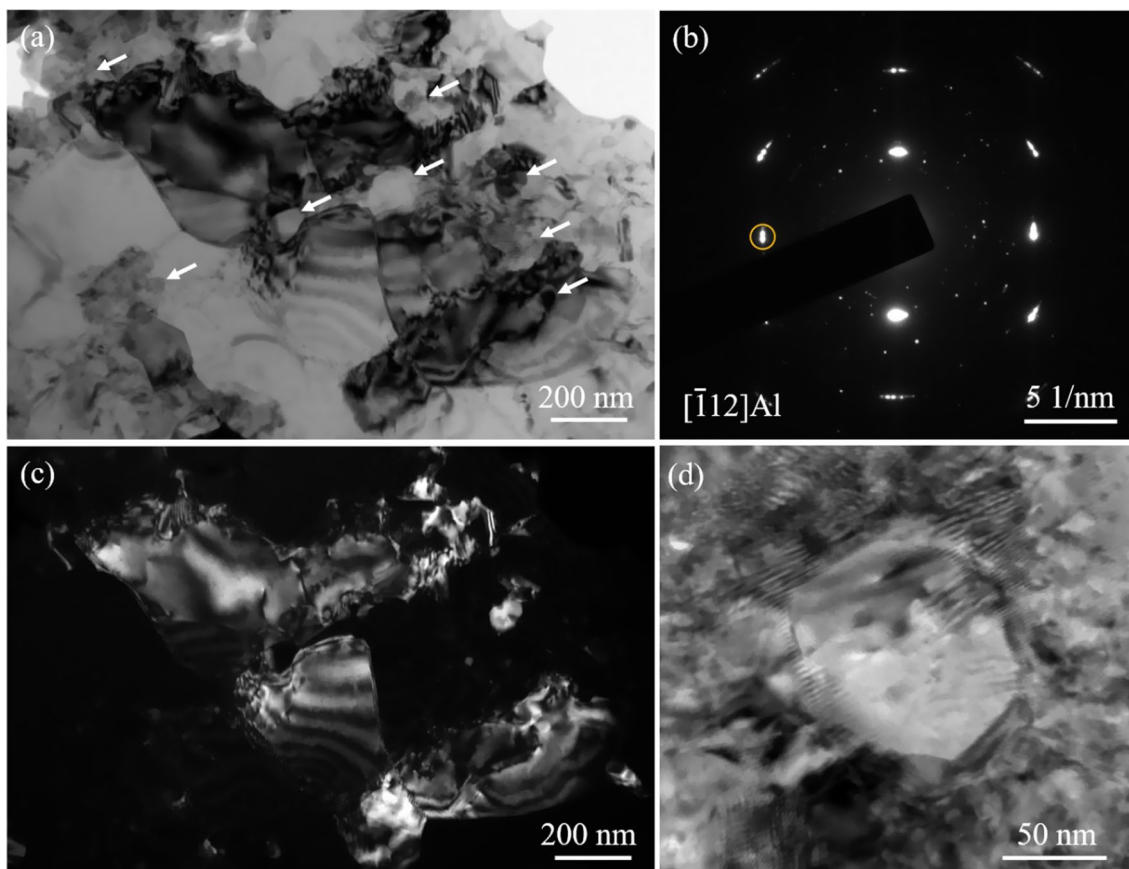
Fig. 4 **a** TEM bright field image of the post-deformation nanocomposite, **b** SAED pattern, **c** TEM dark field image from **a**, the dark field image is obtained using (220) diffraction spot as indicated by orange circle in **b**, **d** a high magnification TEM image of nanoparticle/matrix interface

between Al_2O_3 nanoparticle and secondary dislocations, this will be discussed later. Herein, the contributions from CTE and EM mismatch strengthening can be calculated according to the following Taylor relation [32], respectively: $\Delta\sigma_{GND}^{CTE} = \sqrt{3}\eta\mu_m b\sqrt{\rho_{GND}^{CTE}}$ and $\Delta\sigma_{GND}^{EM} = \sqrt{3}\beta\mu_m b\sqrt{\rho_{GND}^{EM}}$, where $\eta=0.5$ and $\beta=0.7$ are geometric constants, $\mu_m = 26GPa$ refers to the shear modulus of pure Al, and $\rho_{GND}^{GM} = \frac{3\sqrt{2}V_p\varepsilon_p}{\pi b d_p}$ is the GND density due to the EM mismatch, ε_p is the yielding strain. The experimentally measured ρ_{GND}^{CTE} was taken for calculation.

In general, the deformation of particles reinforced Al matrix composite is determined by the interaction of glide dislocations with the particles, grain boundaries and themselves. Especially when the particle size is in a nanometer level, dislocations bypass of nanoparticles through the Orowan mechanism would play a leading role during deformation and make the greatest strengthening contribution [9]. As for the nanocomposite investigated in this study, dislocation pile-ups in arrays distributed along the Al_2O_3 nanoparticles illustrates Orowan strengthening is operative during deformation, as shown in Fig. 4c. A closer look at these TEM images of the post-deformation nanocomposite reveals that deformation subgrains of a grain containing Al_2O_3 nanoparticles are formed. The formation of subgrains having small orientation difference can be further verified by the electron diffraction analysis as shown in Fig. 4b (the SAED pattern corresponding to Fig. 4a), i.e., the diffraction spots are arced and/or even split into several small spots. The well-formed subgrains were formed during the polygonization process dominated by particle-dislocations interaction. This is to say, as dislocations in all sets of active slip planes multiply greatly in terms of particle/matrix interfaces emitting, bypassing of nanoparticles, and entangling with each other, the resultant multiple dislocation pile-ups and tangles around the nanoparticles align themselves to form dislocation cell walls, and then the dislocation cell walls transform into subgrain boundaries by means of dynamically rearranging of dislocations inside the grain [33], thereby reducing the strain energy. As the result, the original coarse grains were polygonized to form subgrains, with low density of dislocations stored inside the subgrains. Thus, the deformation process of the nanocomposite in this study is mainly controlled by dislocation-nanoparticle interactions and consequently the formation of subgrains with small misorientations. A very high density of dislocations on the order of the saturation value is achieved rapidly during the early stage of deformation, with the result that extra high strain hardening rate was observed in the strain hardening rate-true strain curve for the nanocomposite (Fig. 1b). As the strain increases, subgrains are created by dislocations rearrangement, meanwhile, the dislocations inside the subgrains were so greatly annihilated that dislocation density reduce to a

lower level at which less or no hardening is expected [33]. As Fig. 1b shows, slight strain softening occurs at strain of 0.08 until fracture. The strengthening contribution due to the resistance of nanoparticles to dislocation motion is given by the Orowan equation [34]: $\Delta\sigma_{Or} = M\frac{0.4\mu_m b}{\pi\lambda}\frac{\ln(\bar{d}/b)}{\sqrt{1-\upsilon}}$, where $M=3.06$ is the mean orientation factor for fcc metal, $v=0.345$ represents the Poisson's ratio of pure Al, $\lambda = d(V_p^{-1/3} - 1)$ is the interparticle distance, and $\bar{d} = (2/3)^{1/2}d_p$ is the mean diameter of a circular section in a random plane for a spherical particle.

As mentioned above, the strength improvement of the nanocomposite results from grain boundary strengthening, load bearing strengthening, dislocation strengthening, and Orowan strengthening. The respective contributions of these strengthening mechanisms were calculated and summarized in Table 1. It can be found that the Orowan strengthening plays the most important role, which is consistent with the experimental observations. One should be noted that these strengthening mechanisms may interact with each other, showing a synergetic effect to strengthening increase. The overall yield strength of the nanocomposite can be estimated by using a modification of Zhang and Chen method [17]: $\sigma_c = \sigma_m\left(1 + \frac{\Delta\sigma_G}{\sigma_m}\right)\left(1 + \frac{\Delta\sigma_L}{\sigma_m}\right)\left(1 + \frac{\Delta\sigma_{GND}}{\sigma_m}\right)\left(1 + \frac{\Delta\sigma_{Or}}{\sigma_m}\right)$, where $\Delta\sigma_{GND} = \Delta\sigma_{GND}^{CTE} + \Delta\sigma_{GND}^{EM}$. The value estimated for σ_C is 551 MPa, in agreement with the experimental yield stress value.

4 Conclusion

In this study, the strengthening mechanisms of Al matrix nanocomposite with incorporated Al_2O_3 nanoparticles reaching up to 15 vol.% were examined experimentally and modeled analytically. The results demonstrate that the several strengthening mechanisms including grain boundary strengthening, load transfer strengthening, dislocation strengthening due to nanoparticles induced GNDs, and Orowan strengthening contribute to the significant strength improvement of the studied nanocomposite. Among these

Table 1 Predicted results of the strengthening contribution in the as-produced nanocomposite

Strengthening mechanisms	Strengthening (MPa)
Grain boundary	44.7
Load transfer	3.3
CTE mismatch induced GND	16.4
EM mismatch induced GND	42.1
Dislocation bypass of nanoparticle	269.6

strengthening mechanisms, the dislocation strengthening due to the thermal mismatch between Al matrix and Al$_2$O$_3$ nanoparticles becomes insignificant compared with that of nanocomposites reinforced with relatively low volume fraction nanoparticles, this is confirmed by the observation of a low density of thermal mismatch induced GNDs near the Al$_2$O$_3$ nanoparticles, which may be resulted from annihilation of the GND loops of opposite sign between Al$_2$O$_3$ nanoparticles. The Orowan strengthening has the most important contribution to strength increase, due to the fact that the deformation process of the studied nanocomposite is dominated by interactions between Al$_2$O$_3$ nanoparticles and dislocations, i.e., dislocations pile-up around the Al$_2$O$_3$ nanoparticles and stand in line with each other and subsequently form ultrafine subgrains. Additionally, inspection of the respective contribution of these strengthening mechanisms predicted by using theoretical models confirms the significant role of Orowan strengthening in strengthening of the nanocomposite containing high content nanoparticles.

Declarations

Conflict of interest The authors declare that they have no conflict of interest.

References

[1] R. Geng, F. Qiu, Q.C. Jiang, Adv. Eng. Mater. **20**, 1701089 (2018)

[2] Z.H. Zhang, T. Topping, Y. Li, R. Vogt, Y.Z. Zhou, C. Haines, J. Paras, D. Kapoor, J.M. Schoenung, E.J. Lavernia, Scr. Mater. **65**, 652 (2011)

[3] M.J. Li, K.K. Ma, L. Jiang, H. Yang, E.J. Lavernia, L.M. Zhang, J.M. Schoenung, Mater. Sci. Eng. A **656**, 241 (2016)

[4] X. Yao, Z. Zhang, Y.F. Zheng, C. Kong, M.Z. Quadir, J.M. Liang, Y.H. Chen, P. Munroe, D.L. Zhang, J. Mater. Sci. Technol. **33**, 1023 (2017)

[5] D. Poirier, R.A.L. Drew, M.L. Trudeau, R. Gauvin, Mater. Sci. Eng. A **527**, 7605 (2010)

[6] J. Hemanth, Mater. Sci. Eng. A **507**, 110 (2009)

[7] A. Sanaty-Zadeh, Mater. Sci. Eng. A **531**, 112 (2012)

[8] A. Mazahery, H. Abdizadeh, H.R. Baharvandi, Mater. Sci. Eng. A **518**, 61 (2009)

[9] Y.C. Kang, S.L. Chan, Mater. Chem. Phys. **85**, 438 (2004)

[10] H. Su, W.L. Gao, Z.H. Feng, Z. Lu, Mater. Des. **36**, 590 (2012)

[11] A.B. Li, G.S. Wang, X.X. Zhang, Y.Q. Li, X. Gao, H. Sun, M.F. Qian, X.P. Cui, L. Geng, G.H. Fan, Mater. Sci. Eng. A **745**, 10 (2019)

[12] J.L. Liu, X.Y. Huang, K. Zhao, Z.W. Zhu, X.X. Zhu, L.N. An, J. Alloys Compd. **797**, 1367 (2019)

[13] L.N. An, J. Qu, J.S. Luo, Y. Fan, L.G. Zhang, J.L. Liu, C.Y. Xu, P.J. Blau, J. Mater. Res. **26**, 2479 (2011)

[14] L.Y. Chen, J.Y. Peng, J.Q. Xu, H. Choi, X.C. Li, Scr. Mater. **69**, 634 (2013)

[15] J.F. Guo, J. Liu, C.N. Sun, S. Maleksaeedi, G. Bi, M.J. Tan, J. Wei, Mater. Sci. Eng. A **602**, 143 (2014)

[16] J. Liu, Z. Chen, F.G. Zhang, G. Ji, M.L. Wang, Y. Ma, V. Ji, S.Y. Zhong, Y. Wu, H.W. Wang, Mater. Res. Lett. **6**, 406 (2018)

[17] Z. Zhang, D.L. Chen, Scr. Mater. **54**, 1321 (2006)

[18] T.C. Lin, C.Z. Cao, M. Sokoluk, L. Jiang, X. Wang, J.M. Schoenung, E.J. Lavernia, X.C. Li, Nat. Commun. **10**, 4124 (2019)

[19] S. Scudino, G. Liu, K.G. Prashanth, B. Bartusch, K.B. Surreddi, B.S. Murty, J. Eckert, Acta Mater. **57**, 2029 (2009)

[20] S. Scudino, G. Liu, M. Sakaliyska, K.B. Surreddi, J. Eckert, Acta Mater. **57**, 4529 (2009)

[21] M. Yuan, D.C. Zhang, C.G. Tan, Z.C. Luo, Y.F. Mao, J.G. Lin, Mater. Sci. Eng. A **590**, 301 (2014)

[22] C.S. Marchi, F. Cao, M. Kouzeli, A. Mortensen, Mater. Sci. Eng. A **337**, 202 (2002)

[23] M. Rahimian, N. Parvin, N. Ehsani, Mater. Sci. Eng. A **527**, 1031 (2010)

[24] M. Kouzeli, D.C. Dunand, Acta Mater. **51**, 6105 (2003)

[25] T. Sakamoto, S. Kukeya, H. Ohfuji, Mater. Sci. Eng. A **748**, 428 (2019)

[26] M.R. Mattli, P.R. Matli, A. Shakoor, A.M.A. Mohamed, Ceramics **2**, 126 (2019)

[27] B.Y. Cao, S.P. Joshi, K.T. Ramesh, Scr. Mater. **60**, 619 (2009)

[28] R.J. Arsenault, N. Shi, Mater. Sci. Eng. **81**, 175 (1986)

[29] D. Dunand, A. Mortensen, Mater. Sci. Eng. A **135**, 179 (1991)

[30] A.M. Redsten, E.M. Klier, A.M. Brown, D.C. Dunand, Mater. Sci. Eng. A **201**, 88 (1995)

[31] L. Jiang, H. Yang, J.K. Yee, X. Mo, T. Topping, E.J. Lavernia, J.M. Schoenung, Acta Mater. **103**, 128 (2016)

[32] L.H. Dai, Z. Ling, Y.L. Bai, Compos. Sci. Technol. **61**, 1057 (2001)

[33] Y.F. Liu, F. Wang, Y. Cao, J.F. Nie, H. Zhou, H.B. Yang, X.F. Liu, X.H. An, X.Z. Liao, Y.H. Zhao, Y.T. Zhu, Scr. Mater. **162**, 316 (2019)

[34] A. Kelly, R.B. Nicholson, *Strengthening Methods in Crystals* (Elsevier, Amsterdam, 1971), p. 9